XPS Analysis of Passive Film on Stainless Steel

R. Natarajan[1], N. Palaniswamy[2], M. Natesan[*,2] and V.S. Muralidharan[3]

[1]*Alagappa Government Arts College, Karaikudi, TN, India-630003*

[2]*Corrosion Science & Engineering Division, Central Electrochemical Research Institute, Karaikudi, TN, 630006, India*

[3]*Alagappa Chettiar College of Engineering and Technology, Karaikudi, TN, 630004, India*

Abstract: Potentiodynamic, impedance measurements were carried out on 304 stainless steel in 0.5N, 1.0, 2.0 and 5.0 N H_2SO_4 solutions. X-ray photoelectron spectroscopic [XPS] studies carried out on 304 stainless steel in H_2SO_4 solutions revealed the existence of CrOOH, Cr_2O_3, γ-Fe_2O_3, γ- FeOOH, Mn_2O_3, Mn_3O_4, MnS, Ni $(OH)_2$, Ni_2O_3, NiO, sulphides. The passive film found to contain chromium oxide inner layer and the dissolution of iron through it caused the formation of oxides of iron namely γ - Fe_2O_3 and γ-FeOOH. Higher oxides of manganese and nickel are also due to dissolution through the film. Sulphates are reduced to sulphur chemically by the released protons from anodic polarization.

Keywords: 304 stainless steel, passive film, impedance method, polarization, XPS studies.

1. INTRODUCTION

Kier [1] published the first report on the passivity of iron in 1790. In 1925 active-passive behaviour on iron in 60% HNO_3 was demonstrated [2]. The passive film on iron was found to be not an insulator by Faraday [3]. In 1939 passivation of stainless steel was discussed using electronic configuration [4]. Passive state and dissolution were found to be independent of surface film [5]. Ellipsometric studies on 18/8 stainless steel revealed the existence of oxide on iron and found air formed oxide was replaced by a thicker and denser oxide. On progressive anodic polarization, metal form multilayer oxide films with increase in thickness [6]. Hackerman [7] proposed a model for the growth of oxide from initially adsorbed oxygen. In stainless steel, the presence of chromium is responsible for passivation [8], nickel stabilizes austenitic structure [9] and Molybdenum prevents depassivation by pitting [10].

Steel tanks are being used to transport and store sulphuric acids. However for longer storage of time the steel tanks are anodically protected. For transportation of higher concentrations of sulphuric acids stainless steel lined or stainless steel containers are used as the surface become passivated. The present investigation aims at the understanding of the composition of passive film formed on 304 - stainless steel in H_2SO_4 solutions in the primary passive and secondary passive region.

2. MATERIALS AND METHODOLOGY

304 stainless steel rod encapsulated in Teflon with 0.5cm diameter was used as the working electrode for electrochemical studies. The surface of the electrode was polished to mirror finish using SiC emery paper (1/0 to 4/0) degreased with acetone and finally rinsed with triple distilled water. For

XPS studies one sq. cm surfaces were exposed and and analar grade chemicals were used.

Potentiodynamic anodic polarization study was carried out using EG & G Princeton Applied Research (PAR) model 173 potentiostat with EG & G PAR model 175 programmer connected to RiKadenky x-y recorder. The electrochemical cell having a capacity of 200ml with provision for gas inlet, working electrode, counter electrode (Platinum foil having $2cm^2$ area connected with platinum wire dipped in mercury contact through copper wire) and salt bridge were used. The potential of the working electrode was measured with respect to saturated calomel electrode [SCE] which was connected through a salt bridge. After 15 minutes, the IR compensation was done and the experiment was carried out. The scanning potential range was from -500mV to 800mV *vs* SCE at a scan rate of 1mV/sec. Potential was plotted against log current.

Alternating current impedance measurements were carried out by using computer controlled EG&G PAR Model 6310 electrochemical impedance analyzer. The experimental setup was the same as for potentiostatic method. At different preselected potentials, impedance diagrams were obtained. The frequency ranged from 100 mHz to 10 kHz. From the Bode plots (log |z| *vs* log w), the charge transfer resistance) (R_{ct}) and solution resistances (R_s) were calculated. The double layer capacitance (C_{dl}) were calculated from the equation

$$C_{dl} = \tfrac{1}{2}\, \pi \, f_{max} \, R_{ct} \tag{1}$$

where, f_{max} is the maximum frequency obtained in the Nyquist plots.

The chemical composition of the passive film formed on the surface was analysed by using VG scientific mark II ESCA Spectrometer. The film was formed on the surface by keeping the specimen for about an hour in the primary passivation range potential and in secondary passivation range potential in 0.5N and 5.0N H_2SO_4 solutions. The surface was dried and examined. In order to investigate the nature and valencies of the constituent's elements in the film the specimen was analyzed by means of XPS MgK_{α} irradiation with a

*Address correspondence to this author at the Corrosion Science & Engineering Division, Central Electrochemical Research Institute, Karaikudi, TN, 630006, India; Tel: 91-(04565) 227550-9; Fax; (04565) 227713/ 227779; E-mail: mnatesan@rediffmail.com

mean energy of 1253.6 eV. The voltage and current applied to the x-ray tube were 8kV and 100mA respectively. The specimen container was evacuated to 10^{-9} m bar. C_{IS} binding energy, 285 eV of hydrocarbon contamination was used as calibration to compensate the charging system. A delocalized Ar^+ ion beam accelerated under 2KeV was used to remove adsorbed contaminants on the surfaces. The photoelectron as spectra of Fe 2p, Cr 2p, Ni 2P, Mn 2p, S 2p, O 2p electron levels are measured.

3. RESULTS

Potentiostatic anodic polarization studies were carried out on stainless steel in various concentrations of H_2SO_4 solutions (Fig. **1**). Open circuit potential (OCP) became noble with the concentration of H_2SO_4. When polarized anodically, current started increasing upto -370mV in 0.5 N H_2SO_4 solutions ($E_{critical}$). This potential was nearly invariant for all concentrations of H_2SO_4 (Table **1**). Further polarization decreased the current due to the formation of passive film. The primary passivation of the surface occurred in the potential range of -200mV to 0mV. Beyond 0mV, current started rising till the potential reached 50mV. Further anodic polarization caused a secondary passivation. Beyond 350mV, current started increasing due to oxygen evolution. Increase of concentration of the acid increased critical current (i_{crit}), primary passivation current ($i_{p.p}$) and secondary passivation current ($i_{s.p}$).
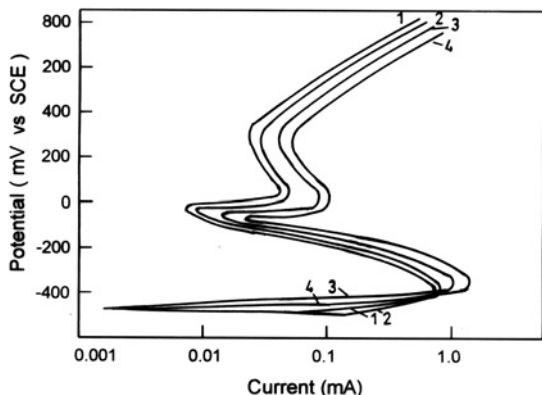
Fig. (1). Anodic polarization curve for stainless steel in various concentrations of H_2SO_4 solutions.

3.1. Open Circuit Potential Region

At the open circuit potential, impedance measurements were made. The obtained Bode plots (Fig. **2**) revealed that the shapes of curves are similar. The charge transfer resistances, solution resistances and double layer capacitances were calculated (Table **2**). Charge transfer resistances decreased and double layer capacitance (C_{dl}) increased with the concentration of H_2SO_4.
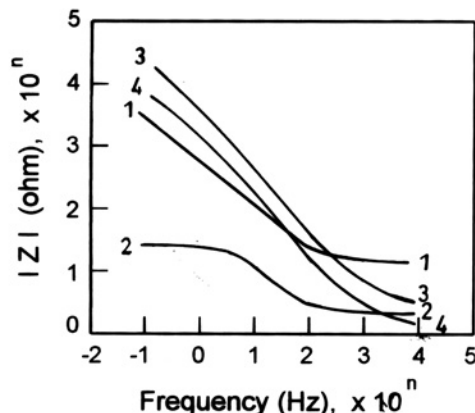
Fig. (2). Bode plots obtained for stainless steel in various concentrations of H_2SO_4 solutions at the open circuit potential region (- 450mV).

Table 2. Parameters Derived from Impedance Diagrams for Various Concentrations of H_2SO_4 at the Open Circuit Potential

Concentration of H_2SO_4 (Normality)	Charge Transfer Resistance k. ohm/cm^2	Double Layer Capacitance F/cm^2 x 10^{-4}
0.5	24.74	2.17
1.0	21.16	6.39
2.0	7.33	7.54
5.0	2.19	16.3

3.2. Active Dissolution Region

Fig. (**3**) presents the Bode plots obtained in various concentrations of H_2SO_4 at -400mV. The curves exhibited longer horizontal regions at lower frequencies suggesting the absence of a passive film. Increase of acid concentration decreased the horizontal regions. Charge transfer resistances decreased while double layer capacitance increased with acid concentration (Table **3**).

Table 1. Parameters Derived from Anodic Polarization Curves in Various Concentration of H_2SO_4 Solutions

Concentration of H_2SO_4 (Normality)	OCP mV *vs* SCE	Critical Range		Primary Passivation Range		Secondary Passivation Range	
		Potential mV *vs* SCE	Current 10^{-4} A/cm^2	Potential mV *vs* SCE	Current 10^{-6} A/cm^2	Potential mV *vs* SCE	Current 10^{-4} A/cm^2
0.5	-450	-370	7	-100	8.6	350	3.8
1.0	-420	-370	8.5	-80	9.2	350	5.1
2.0	-400	-350	9.2	-60	12	350	7.5
5.0	-380	-350	12	-50	40	350	9.0
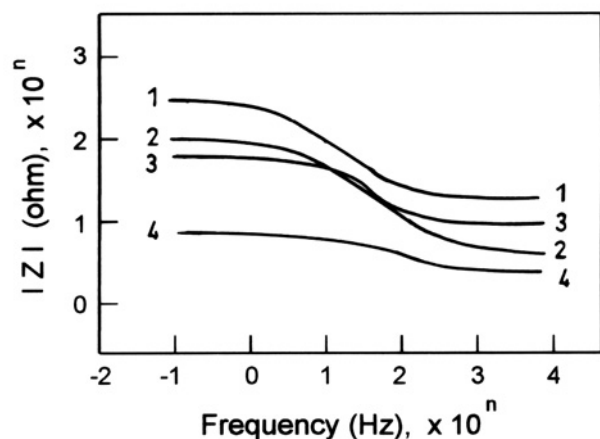
Fig. (3). Bode plots obtained for stainless steel in various concentrations of H_2SO_4 at active potential region (-400mV).

Table 3.   Parameters Derived from Impedance Diagrams for Various Concentrations of H_2SO_4 at -400 mV (Active Dissolution Range)

Concentration of H_2SO_4 (Normality)	Charge Transfer Resistance k. ohm/cm^2	Double Layer Capacitance F/cm^2 x 10^{-3}
0.5	291	3.6
1.0	102	3.9
2.0	55	6.2
5.0	7	7.0

3.3. Primary Passivation Region

When the log impedance was plotted against log frequency (Bode plots) in the primary passivation region at -100mV, the vertical region increased with H_2SO_4 concentration (Fig. **4**) Solution resistance decreased with H_2SO_4 concentration. The lower primary passivation charge transfer resistance values are due to the less stable newly formed thin film. Capacitance of the double layer increased with acid concentration (Table **4**).
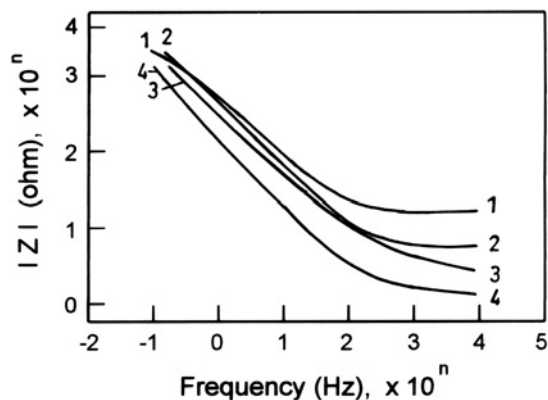
Fig. (4). Bode plots obtained for stainless steel in various concentrations of H_2SO_4 at the primary passivation region. (-100mV).

Table 4.   Parameters Derived from Impedance Diagrams for Various Concentrations of H_2SO_4 at -100 mV (Primary Passivation Range)

Concentration of H_2SO_4 (Normality)	Charge Transfer Resistance k. ohm/cm^2	Double Layer Capacitance F/cm^2 x 10^{-4}
0.5	3.4	4.50
1.0	3.2	5.60
2.0	2.1	7.54
5.0	1.3	7.50

The XPS pattern obtained on the protection film formed in 0.5N H_2SO_4 at -100mV is shown as Fig. (**5**). The binding energies of all elements and their compounds are referred to using standard tables published by VG-XPS instrumentation Co., Ltd., The peaks at 574.0eV and 586.03 eV are due to the presence of 2p $_{3/2}$ and 2p ½ electrons of chromium atom in Cr^o state. Peaks at 576.4 eV and 586.38 eV are due to the presence of 2p $_{3/2}$ and 2p ½ electrons of chromium atom in $Cr(OH)_3$. Peaks at 577.6eV, 578.6eV and 588.0 eV, 586.03 eV by chromium 2p $_{3/2}$ and 2p ½ electrons denote the presence of chromium as Cr_2O_3. The peak at 579.0 eV is due to the presence of 2p $_{3/2}$ electrons of chromium atoms in CrOOH. The peak at 580.1 eV noticed by 2p $_{3/2}$ electrons of chromium is due to CrO_3. The same binding energy for Cr 2p $_{3/2}$ was observed earlier [11-16]. The peak at 719.92 eV is due to the presence of iron 2p $_{3/2}$ electron which indicates the free iron. Iron peaks observed at the binding energies of 707.0 eV and 708.7 eV are due to the presence of its $2p_{3/2}$ and 2p½ electrons which represent Fe^{2+} and Fe^{3+} states as oxide. The peaks at 706.82 eV and 723.98 eV indicate $2p_{3/2}$ and 2p½ electron of iron as Fe_3O_4 and $Fe(OH)_3$. The peaks at 274.30 eV and 725.27 eV indicate iron in $2p_{3/2}$ state and thus α-Fe_2O_3. The peaks at 710.9 eV and 711.60 eV by Fe 2p½ electron indicate γ-FeOOH. The peaks at 724.97 eV and 711.44 eV are due to Fe $2p_{3/2}$ and Fe 2p ½ electron level. These peaks denote the presence of α-FeOOH. The binding energies for iron and iron compounds observed in the present study are in conformity with earlier work. The peak observed at 638.76 eV indicates Mn in $2p_{3/2}$ state. The peaks at 641.12 eV and 640.64 eV suggest Mn 2p½ electrons in Mn_2O_3 and Mn^{4+} species. The peaks at 642.2 eV, 641.0 eV and 640.1 eV suggest Mn $2p_{3/2}$ electrons. These indicate manganese as Mn_2O_3, Mn_3O_4 and MnS respectively. MnS existence is inferred from peak at 640.3 eV. The observed binding energies at 852.8 eV, 854.0 eV, 856.5 eV, 854.1 eV, 856.9 eV and 854.9 eV suggest Ni $2p_{3/2}$ electrons and nickel existence as Ni, NiO, $Ni(OH)_2$, Ni_2O_3 and NiO respectively. The binding energies for nickel and its oxides has been observed earlier confirm this [17-22]. The peaks obtained at 530.1 eV, 531.5 eV, 533.0 eV suggest oxygen in 1s½ state and suggest oxygen to be present as O^{2-}, OH^- and $H_2O – SO_4^{2-}$ respectively. The binding energies correspond to 162.4 eV and 169.0 eV suggest the existence of sulphur in 2S ½ state may be as S^{2-} and SO_4^{2-} respectively.

Fig. (**8**) presents the XPS patterns of the film formed from 5.0 N H_2SO_4 solutions at -50mV. The appearance of a peak at 574.0 eV indicates Cr^o and Cr $2p_{3/2}$ states. The peaks
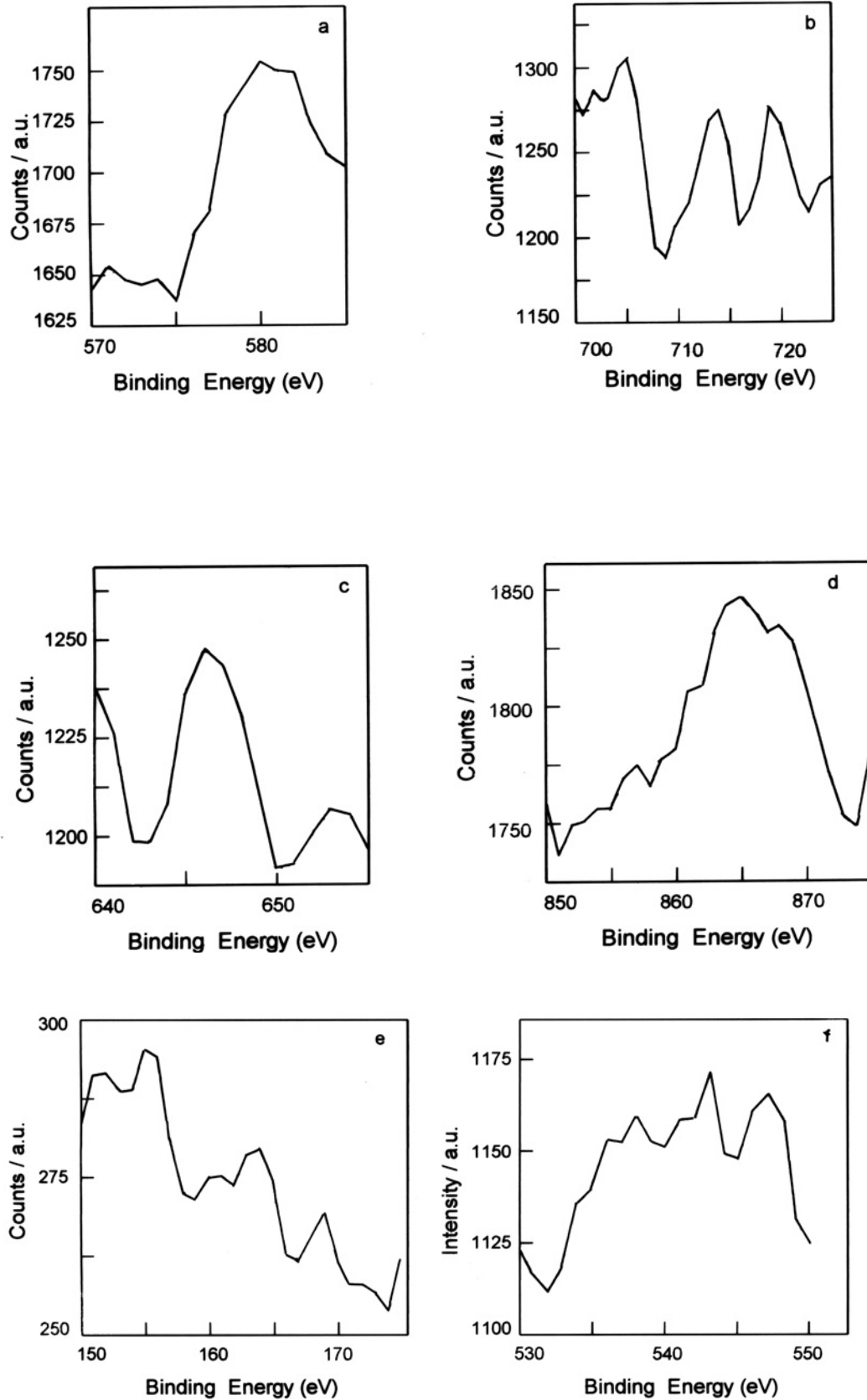
Fig. (5). XPS pattern obtained from primary passive layer of stainless steel in 0.5N H_2SO_4. (at -100 mV). (**a**) chromium, (**b**) iron, (**c**) manganese, (**d**) nickel, (**e**) sulphur and (**f**). oxygen.

observed at 576.4 eV and 578.6 eV indicate $Cr2p_{3/2}$ electrons and Cr_2O_3 presence in the film. The peaks at 577.6eV and 586.38 suggest Cr $2p_{3/2}$ and Cr $2p_{1/2}$ core electrons. These peaks denote the presence of Cr $(OH)_3$, Cr $2p_{3/2}$ core electron as indicated by the peak at 579.0eV suggesting the presence of CrOOH. The existence of CrO_3 was inferred from a peak at 580.1eV.

The $Fe2p_{3/2}$ electron gave the peaks at 706.82eV, 710.97 eV, 711.60eV and 711.44eV. These peaks indicate the presence of Fe_3O_4, αFe_2O_3, γ-FeOOH and α-FeOOH respectively. The existence of Fe_3O_4, Fe, α-Fe_2O_3, γ-FeOOH and α-FeOOH is inferred from $Fe2p_{3/2}$ electrons at 723.98 eV, 719.92 eV, 724.30eV, 725.2 eV and 724.97 eV.

The peaks observed at 638.76.eV, 641.12 eV and 642.2 eV are due to $Mn2p_{3/2}$ electrons. These indicate the existence of Mn^o, Mn $(OH)_3$, Mn_2O_3 and MnO_2. The peaks appeared at 852.8 eV, 854.0eV, 856.5eV, 854.9eV, 856.9eV and 854.9eV are due to Ni $2p_{3/2}$ electrons suggesting Ni, NO, $Ni(OH)_2$, NiS, Ni_2O_3 and NiO respectively. The existence of S^{2-} and SO_4^{2-} species are inferred from the peaks at 162.4 eV and 169.4eV. The oxygen species O^{2-}, OH^-, H_2O-SO_4^{2-} are inferred from the peaks at 530.2eV, 531.4eV and 532.9eV. The peaks at 530.17eV, 529.98eV, 530.2eV, 530.3eV, 529.98eV, 530.85eV and 530.01eV suggest O1s $\frac{1}{2}$ electron and O-M bonds, Fe_3O_4, α-Fe_2O_3, γ-FeOOH, α-FeOOH, Cr_2O_3, $Cr(OH)_3.0.4$ H_2O and CrO_3 respectively. The peak at 531.4eV is due to O1 S $\frac{1}{2}$ electron in γ-FeOOH and α-FeOOH.

3.4. Secondary Passivation Range

Fig. (**6**) presents the Bode plots in different concentrations obtained at 350mV (secondary passivation range). The horizontal region at higher frequency is not sharp. There is not much variation in the slopes of the vertical portions. The charge transfer resistances are higher compared to those obtained in primary passivation range and C_{dl} values are lower (Table **5**).
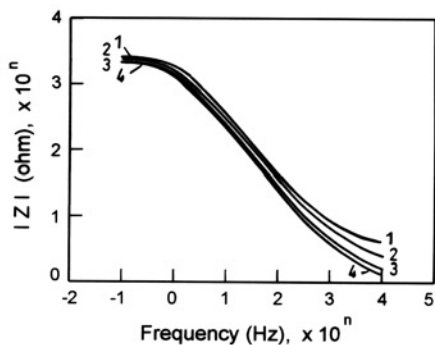
Fig. (6). Bode plots for stainless steel in various concentrations of H_2SO_4 obtained at secondarypassive potential region. (350mV).

Fig. (**7**) presents XPS patterns observed on the surface kept at 350mV in 0.5H H_2SO_4. The observed peaks at 578.6eV and 579.0eV suggest the presence of chromium as $2p_{3/2}$ electrons and Cr_2O_3 or CrOOH on the surface film. The peaks at 586.03 eV, 586.38eV and 588.0eV suggest the presence of chromium as Cr_2O_3, Cr $(OH)_3$ and CrO_3 respectively.

The presence of FeO and Fe^{3+} state with film was inferred from the peaks obtained at 708.7eV and 707.0eV respectively. The peaks at 710.6eV corresponding to $Fe2p_{3/2}$ indicate the presence of Fe $(OH)_3$. Fe_3O_4 presence is indicated by 706.82eV ($Fe2p_{3/2}$) and 723.9eV ($Fe2p_{1/2}$). The peaks at 724.30 eV and 725.27eV indicate α-Fe_2O_3 in the film. The peak at 710.9eV given by $Fe2p_{1/2}$ core electron denotes the presence of γ-FeOOH. The presence of α-FeOOH is indicated by the peaks at 724.97eV and at 711.44eV ($Fe2p_{3/2}$ and $Fe2p_{1/2}$ core electrons). The peaks obtained at 638.76 eV, 641.12eV, 640.64eV and 642.2eV are due to Mn $2p_{3/2}$ electrons. The film may contain Mn^o, Mn^{3+}, and $Mn4^+$ species. The existence of Mn_2O_3, Mn_3O_4 and MnS are inferred by $Mn2p_{1/2}$ electrons as revealed by the peaks at 642.2eV, 641.0eV and 640.3eV. Nickel may be present as Ni^o, Ni^{2+} in NiO and $Ni(OH)_2$ as suggested by the peaks at 852.8eV, 854.0eV, 856.5eV, 854.1eV, 856.9eV and 854.9eV. Sulphur may be present in the film as S^{2-} as revealed by the observed peak at 162.4eV.

Table 5.   Parameters Derived from Impedance Diagrams for Various Concentrations of H_2SO_4 at +300 mV (Secondary Passivation Range)

Concentration of H_2SO_4 (Normality)	Charge Transfer Resistance k. ohm/cm^2	Double Layer Capacitance F/cm^2 x 10^{-4}
0.5	13.6	1.20
1.0	13.2	1.25
2.0	13.0	1.70
5.0	9.4	2.30

Fig. (**9**) presents the XPS spectra obtained in the secondary passivation range (at350 mV) in 5.0N H_2SO_4. The peaks at 576.03eV, 586.38eV, 588.3e are due to Cr $2p_{3/2}$ and the peaks at 586.0-3eV, 586.38eV and 588.32eV are due to $Cr2p_{1/2}$. These suggest the presence of Cr_2O_3, $Cr(OH)_3$. 0.4 H_2O, CrO_3 respectively. $Cr2p_{3/2}$ electron gives rise to peaks at 579.8eV and suggests CrOOH in the film. The peaks at 710.95eV, 710.97eV and 711.60eV suggest Fe $2p_{3/2}$ electrons and Fe_3O_4, α-Fe_2O_3, γ-FeOOH presence in the film. Fe 2 P $\frac{1}{2}$ electrons gave rise to the peaks at 723.98eV, 724.30eV and suggest the incorporation of Fe_3O_4 and α Fe_2O_3 in the film. The peaks at 642.2 eV, 641.8eV suggest $Mn2p_{1/2}$ electrons and MnO_2 and MnS in the film. The peaks at 852.8eV, 854.0eV, 856.5eV, 854.1eV, 856.9eV and 854.9eV suggest Ni $2p_{3/2}$ electrons and the presence of Ni^o, NiO, $Ni(OH)_2$, NiS, Ni_2O_3, NiO respectively. The peaks at 529.98eV, 531.4eV and 533.0eV suggest O1s $\frac{1}{2}$ electron and the presence of M-O, OH^-, H_2O-SO_4^{2-} in the film respectively. The presence of S^{2-} and SO_4^{2-} in the film was inferred from the S2 P$\frac{1}{2}$ peaks at 162.4eV and 169.0eV.

3.5. Transpassive Region

Fig. (**10**) presents the Bode plot obtained in the transpassive region at 600mV. The charge transfer resistances decreased while the double layer capacitances increased. Enhanced double layer capacitance is due to the adsorption of oxygen atom on the surface of the film (Table **6**).
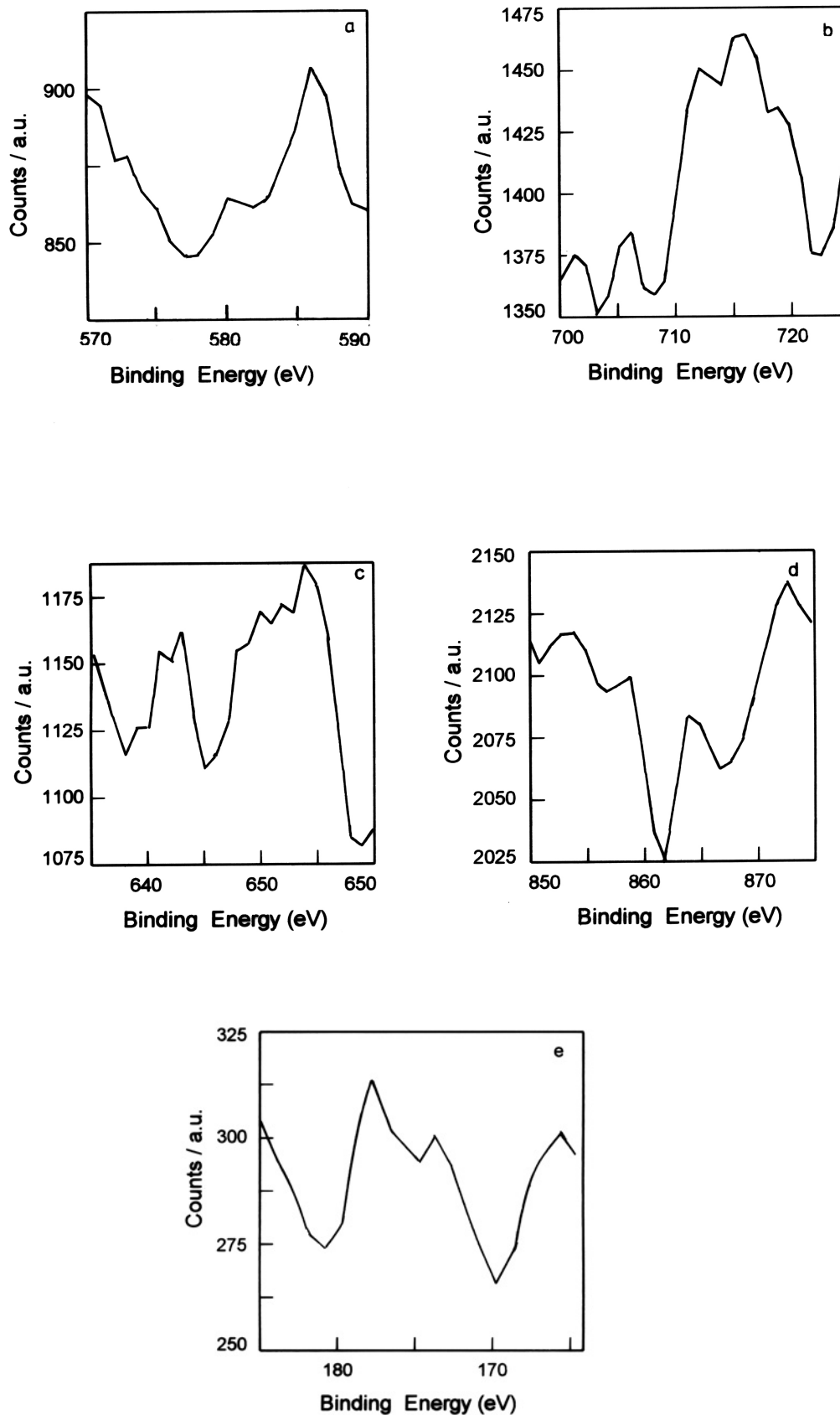
Fig. (7). XPS pattern obtained from secondary passive layer of stainless steel in 0.5N H_2SO_4. (at 350 mV). (**a**) chromium, (**b**) iron, (**c**) manganese, (**d**) nickel, and (**e**) oxygen.
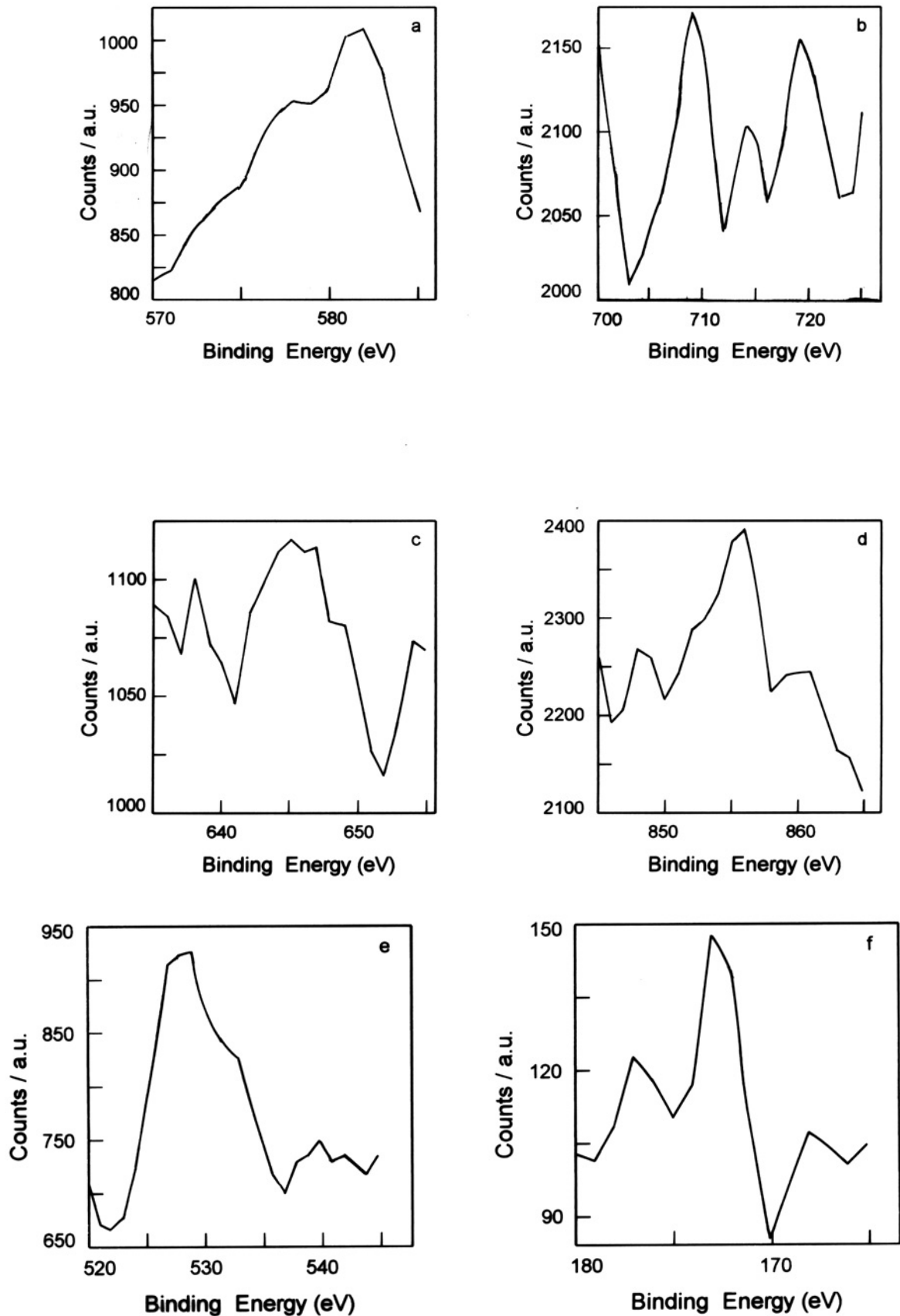
Fig. (8). XPS pattern obtained from primary passive layer of stainless steel in 5.0N H_2SO_4 (-50 mV). (**a**) chromium, (**b**) iron, (**c**) manganese, (**d**) nickel, (**e**) oxygen and (**f**) sulphur.
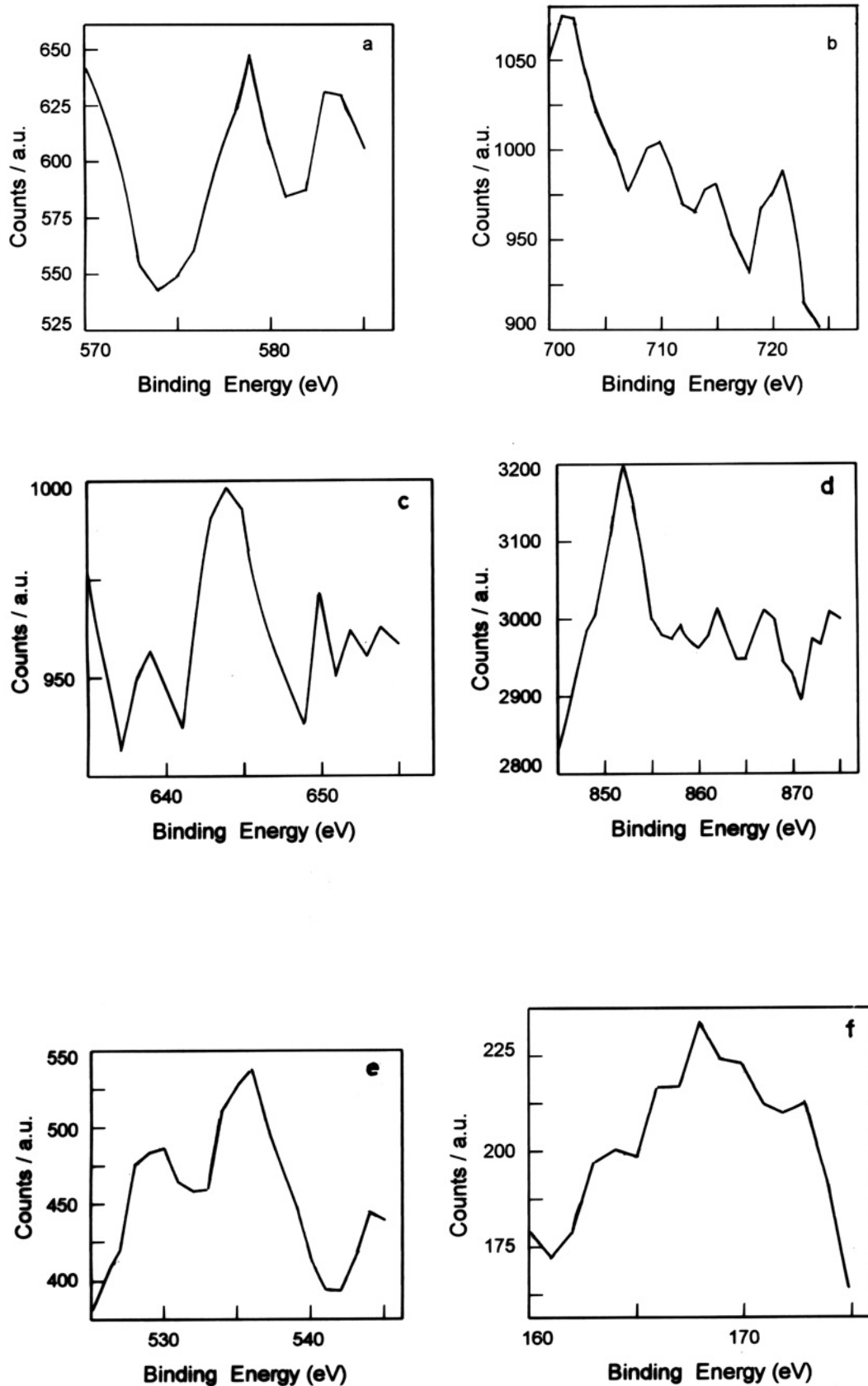
Fig. (9). XPS pattern obtained from secondary passive layer of stainless steel in 5.0N H_2SO_4 (350 mV). (**a**) chromium, (**b**) iron, (**c**) manganese, (**d**) nickel, (**e**) oxygen and (**f**) sulphur.
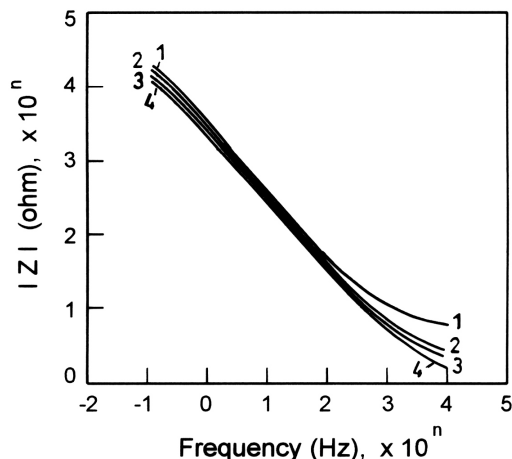
Fig. (10). Bode plots for stainless steel in various concentrations of H_2SO_4 obtained at trans-passive potential region. (450mV).

4. DISCUSSION

Dissolution, passivation and depassivation on metals has been reviewed [23-25]. In general dissolution of metal occurs as

$$M + OH^- \rightleftharpoons MOH^-_{ads} + e \qquad (2)$$

$$MOH^-_{ads} \rightleftharpoons MOH_{ads} + e \qquad (3)$$

$$MOH_{ads} \rightarrow M^{2+} + OH^- \qquad (4)$$

The adsorbed intermediates cover the surface (θ_{MOH}). The film formation may occur directly or indirectly. In indirect film formation, the film nucleation occurs in the solution while in the direct film formation it takes place on the surface. The dissolution precipitation mechanism is covered by metal dissolution, prepassivating film formation and film growth at higher potentials.

In the present study the observed peaks at 530.1eV, 531.5eV and 533.0eV suggest the presence of oxygen as O^{2-} and OH^- ions. Water is bound inside the film. The desorption and dehydration of water molecules favour the film growth. The film may contain M-H_2O bonds as H_2O-M-H_2O, HO-M-OH or O-M-O. Depending upon the anodic potential, film grows. The film on stainless steel was found earlier to be polycrystalline [26]. Sulphate ions adsorb on the surface and favour H_2O-SO_4^{2-} bonds. On Fe-Cr (13%) alloy, the passive film was found to contain hydrated chromium hydroxide on the inner chromium rich inner layer, OH^- ions and adsorb water molecules on this inner layer. In H_2SO_4/Na_2SO_4 solutions, the film contained iron oxide, hydroxide and chromium [27, 28]. In the present study in the primary passivation range Cr_2O_3, CrOOH species were identified.

Table **7** summarizes species identified in the primary and secondary passive region on the film. XPS studies revealed an enrichment of chromium the passive film in the primary range in 0.5N H_2SO_4 while increase of acid concentration favoured iron enrichment in the secondary passive range. Oxides enrichment was higher in dilute acid. Film formation required less coulombs of electricity in dilute acid. Higher acid concentration favoured dissolution. Qualitatively oxides

of chromium, iron and nickel were found to be more in the primary passivation range than in the secondary passivation range.

Table 6. **Parameters Derived from Impedance Diagrams for Various Concentrations of H_2SO_4 at 600 mV (Transpassive Region)**

Concentration of H_2SO_4 (Normality)	Charge Transfer Resistance k. ohm/cm^2	Double Layer Capacitance F/cm^2 x 10^{-5}
0.5	22.6	7.2
1.0	18.3	8.2
2.0	16.1	9.5
5.0	13.6	12.0

Table 7. **Summary of the Compounds Likely to be Present in the Passive Film – XPS Study**

Primary Passivation Range	Secondary Passivation Range
CrOOH, Cr_2O_3, CrO_3	Cr_2O_3, $Cr(OH)_3$, CrO_3
γ-Fe_2O_3, γ FeOOH	$Fe(OH)_3$, α-Fe_2O_3, γ FeOOH
Mn_2O_3, Mn_3O_4, MnS	Fe_3O_4, α-FeOOH
$Ni(OH)_2$, Ni_2O_3, NiO	Mn_2O_3, Mn_3O_4, MnS, MnO_2
S^-, SO_4^{2-}	NiO, $Ni(OH)_2$
	S^{2-}, SO_4^{2-}

Dissolution of iron in H_2SO_4 was found to occur as [29],

$$Fe + H_2O \rightleftharpoons FeOH + H^+ + e \qquad (5)$$

$$FeOH \rightarrow FeOH^+ + e \qquad (6)$$

$$FeOH^+ \rightarrow Fe^{2+} + OH^- \qquad (7)$$
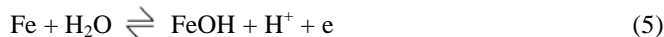
It is known that in 1M sulphate and 1M chloride solutions iron dissolved with the formation of $Fe(OH)_{2\ ads}$. [30].

In the present anodic polarization, iron dissolves through Cr_2O_3 film and reacted with H_2SO_4 to form FeOH, Fe^{2+} species.

$$Fe\ OH + OH^- \rightarrow Fe(OH)_2 + e \qquad (8)$$
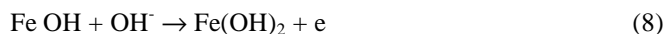
The passive film formation may occur directly or indirectly. In indirect film formation the film nucleation occurs in solution (Classical dissolution precipitation model) while direct film formation theories assert that the film nucleation takes place directly at the solid surface.

$$Fe(OH)_2 + OH^- \rightarrow Fe(OH)_3 + e^- \qquad (9)$$
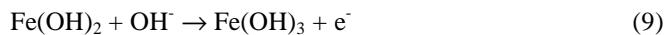
which may undergo structural changes to α-Fe_2O_3

$$2Fe(OH)_3 \rightarrow \alpha\text{-}Fe_2O_3 + 3H_2O \qquad (10)$$

and further anodic polarization favours

$$2Fe(OH) + Fe(OH)_2 \rightarrow Fe_3O_4 + 4H^+ + 4e \qquad (11)$$
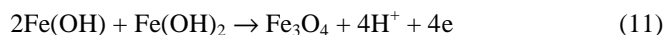
The observed peaks at 706.82eV and 723.98eV confirm the presence of $Fe(OH)_3$. The presence of α-Fe_2O_3 was confirmed by the peaks at 724.30eV and 725.27eV. α-FeOOH presence was indicated by the peaks at 724.97 eV and 711.44eV.

It was shown that a surface of stainless steel exposed to deaerated 1 M H_2SO_4 + 0.5 M HCl solution [31] on anodic polarization, the surface was found to contain surface Cr-rich oxide film responsible for maintaining passivity of stainless steel. This enrichment of Cr in the passive film of Fe–Cr alloys and stainless steel was due to both the lower mobility of Cr in the film and the preferential dissolution of iron into the electrolyte. The Cr-rich film was suggested to consist of a hydrated form of CrOOH [32, 33], while Olefjord claimed that Cr_2O_3 was the main passivating compound [34]. In the initial passivating process, it was suggested that Cr directly reacts with water to form Cr_2O_3, followed by the formation of $Cr(OH)_3$ at the oxide-solution interface. The iron-oxyhydroxide or iron hydroxide appears to be formed with $Cr(OH)_3$, resulting in the formation of a duplex hydroxide layer [35]. On the chromium oxide, the dissolved iron formed oxide like $\alpha.Fe_2O_3$ and Fe_3O_4. Further polarization enriches the chromium content in the film. The nature of the semi conducting passive film changes on polarization [31]. Changes in double layer capacitances with acid concentration and anodic potentials suggest that the transition occurs from n-type to p-type conductivity [36]. Photo electrochemical studies in $0.05M\ H_2SO_4$ revealed that the protective property of the film depends on chromium content in the alloy [37-39].

In the present study chromium enrichment favoured protection and increase of acid concentration enhanced iron dissolution through the film (Table **1**). At moderate anodic potentials, nickel and manganese dissolve to from their oxides. Sulphides incorporation in the film may also arise as the 304-SS alloy contains 0.026 weight % of sulphur. Sulphates may also be reduced by the protons released during polarization (chemical reaction).

In the transpassive region, oxygen evolution may occur on an oxide surface as

$$H_2O \rightleftharpoons OH_{ads} + H^+ + e \qquad (12)$$

$$OH^- + OH_{ads} \rightleftharpoons O^-{}_{ads} + H_2O \qquad (13)$$

$$O^-{}_{ads} \rightleftharpoons O_{ads} + e \qquad (14)$$

$$2O_{ads} \rightleftharpoons O_2 \uparrow \qquad (15)$$

The oxygen evolution from an oxide film involves the participation of adsorbed oxygen atom. If the desorption of oxygen atom is slow, there would be accumulation of oxygen on the surface which changed the double layer capacitance (Table **5**).

5. CONCLUSION

XPS studies carried out on 304 stainless steel in H_2SO_4 solutions revealed the existence of CrOOH, Cr_2O_3, γ-Fe_2O_3, γ-$FeOOH$, Mn_2O_3, Mn_3O_4, MnS, $Ni(OH)_2$, Ni_2O_3, NiO, sulphides on the oxide - environment interface. The passive film was found to contain chromium oxide inner layer and the dissolution of iron through this caused the formation of oxides of iron namely α- Fe_2O_3 and γ-FeOOH. Higher oxides of manganese and nickel are also due to the dissolution through the film. Sulphates are reduced to sulphur chemically by the released protons from anodic polarization.

REFERENCES

[1]   Kier J. Passivity of iron. Phil Trans 1790; 80: 359.

[2]   Lillie RS. Factors affecting transmission and recovery in the passive iron nerve model. J Gen Physiol 1925; 7: 473-507.

[3]   Faraday M. Experimental Research in Electricity. Dover Publ: New York; Reprinted 1965; vol. 2: pp. 234-50.

[4]   Uhlig HH, Wulff J. Trans AIME 1939; 135: 494.

[5]   Blanc A, La Z. Electrochem 1900; 6: 472.

[6]   Transtand L, Borgman CW. Some optical observation on the passivity of iron and steel in nitric and chromic acids. Trans Faraday Soc 1934; 30: 349-66.

[7]   Hackerman N. Sorption, oxidation and passivity. Z Electrochem 1958; 62: 632-7.

[8]   Brookes HC, Graham FJ, Bayles JW. Nucleation and growth of anodic films on stainless steel alloys I. Influence of minor alloying elements and applied potential on passive film growth. J App Electrochem 1990; 20(2): 223-30.

[9]   Zhang BP *etal.* The corrosion behavior of amorphous Ni-Cr-19p alloys in hydrochloric acid. Corros Sci 1992; 33: 667-79.

[10]   Scarberry RC, Gravir DL, Stephens CD. Alloying for corrosion control properties and benefits of alloy material. Mater protec 1967; 6: 54-7.

[11]   Mazurkiewicz B. Anodic passivity of iron in sulphuric acid. Electrochim Act 1993; 38: 495-502.

[12]   Haupt S, Strehblow HH. A combined surface analytical and electrochemical study of the formation of passive layers on Fe/Cr alloys in 0.5 M H_2SO_4. Corros Sci 1995; 37: 43-54.

[13]   Oblonsky LJ, Devine TM. A surface enhanced Raman spectroscopic study of the passive films formed in borate buffer on iron, nickel, chromium and stainless steel. Corros Sci 1995; 37: 17- 41.

[14]   Amaral ST, Muller IL. Effect of silicate on passive films anodically formed on iron in alkaline solution as studied by electrochemical impedance spectroscopy. Corrosion 1999; 55: 17-23.

[15]   Mansfeld F. Electrochemical impedance Spectroscopy (EIS) as a new tool for investigating methods of corrosion protection. Electrochem Act 1990; 35: 1533-44.

[16]   Asami K, Hashimoto K. The X-ray photo-electron spectra of several oxides of iron and chromium. Corros Sci 1977; 17: 559-70.

[17]   Moulder JF, Stickle WF, Sobel PE. Handbook of x-ray photo electron Spectroscopy. Perkin Elmer Corporation Eden Parouine; Minnesota: 1995.

[18]   Brundle CR, Chuang TJ, Wandelt K. Core and valence level photoemission studies of iron oxide surfaces and the oxidation of iron. Surf Sci 1977; 68: 459-68.

[19]   Ikemoto I, *et al.* X-ray photoelectron spectroscopic studies of Cr_2O_3 and some related chromium compounds. J Solid State Chem 1976; 17: 425-30.

[20]   Lu YC, Clayton CR, Brooks AR. A bipolar model of the passivity of stainless steels-II. The influence of aqueous molybdate. Corros Sci 1989; 29: 863-80.

[21]   Marcus P, Olefjord I, Oudar J. The influence of sulphur on the dissolution and the passivation of a nickel-iron alloy-II. Surface analysis by ESCA. Corros Sci 1984; 24: 269-78.

[22]   Olefjord I, Elfstrom BO. The composition of the surface during passivation of stainless steel. Corrosion 1982; 38: 46-52.

[23]   Jayalakshmi M, Muralidharan VS. Sulphur induced depassivation of transition metals in alkali solutions. Corros Rev 1994; 12: 359-75.

[24]   Jayalakshmi M, Muralidharan VS. Empirical and deterministic model of pitting corrosion – on overview. Corros Rev 1996; 14: 375-402.

[25]   Jayalakshmi M, Muralidharan VS. Role of anions in the dissolution passivation and pitting of metals-a review. Corros Rev 2003; 21: 327-47.

[26]   Clayton CR, Doss K, Warren JB. Passivity of metals and semiconductors. Froment M, Ed. Elsevier Bombannes: 1983; 585-90.

[27]   Asami K, Hashimoto K, Shimodaira S. An XPS study of the passivity of a series of iron-chromium alloys in sulphuric acid. Corros Sci 1978; 18: 151-60.

[28]   Castle JE, Clayton CR. The use of in the x-ray photo-electron spectroscopy analyses of passive layers on stainless steel. Corros Sci 1977; 17: 7-26.

[29]   Bockris JOM, Drazic D, Despic AR. The electrode kinetics of the deposition and dissolution of iron. Electrochim Act 1961; 4: 325-61.

[30]   Ogura KA. Dissolution-precipitation model for metal passivation. Electrochem Act 1980; 25: 335-9.

[31] Hermas AA. Polarisation of low phosphorus AISI 304 Stainless steel in sulphuric acid containing arsenites. Br Corros J 1999; 34: 132-8.

[32] Asami K, Hashimoto K, Shimodaira S. An ESCA study of the Fe^{2+}/Fe^{3+} ratio in passive films on iron-chromium alloys. Corros Sci 1976; 1: 387-91.

[33] Sugimoto K, Sawada Y. The role of molybdenum additions to austenitic stainless steels in the inhibition of pitting in acid chloride solutions. Corros Sci 1977; 17: 425-45.

[34] Olefjord I, Brox B. Quantitative ESCA analysis of the passive state of an Fe-Cr-alloy and Fe-Cr-Mo alloy, ibid (26), Passivity of Metals and Semiconductors. Elsevier; Amsterdam: 1983; 561.

[35] Schmuki P, Bohni H, Mansfeld F. A Photoelectrochemical investigation of passive films formed by alternating voltage passivation. J Electrochem Soc 1993; 140: L119.

[36] Yang MZ, Luo JL, Patchet BM. Correlation of hydrogen-facilitated pitting of AISI 304 stainless steel to semiconductivity of passive films. Thin Solid Films 1999; 354: 142-7.

[37] Duret-Thual C, Barrau F. Modification of passive films. Marcus P, Baroux B, Keddam M, Eds.; European Federation of Corrosion. Inst mater 1993; Vol. 12: pp. 176-88.

[38] Okamoto G. Passive film of 18.8 stainless steel structure and its function. Corros Sci 1973; 13: 471-89.

[39] Cigada A, Singaglia D, Re G, Borile F. Contribution to the interpretation of current maxima in the passivity range of Austenitic Stainless steel. Corrosion 1978; 34: 407-10.